Acta Crystallographica Section B
Structural Science
ISSN 0108-7681

Mechanism of the first-order phase transition of an acylurea derivative: observation of intermediate stages of transformation with a detailed temperature-resolved single-crystal diffraction method

Daisuke Hashizume,[a]*† Naoko Miki,[a] Toshiyuki Yamazaki,[a] Yosuke Aoyagi,[a] Tomokuni Arisato,[b] Hiroki Uchiyama,[b] Tadashi Endo,[b] Masanori Yasui[a] and Fujiko Iwasaki[a]

[a]Department of Applied Physics and Chemistry, The University of Electro-Communications, Chofugaoka, Chofu, Tokyo 182-8585, Japan, and [b]Department of Chemistry, Aoyama Gakuin University, Fuchinobe, Sagamihara, Kanagawa 229-8551, Japan

† Present address: Molecular Characterization Division, RIKEN (The Institute of Physical and Chemical Research), Hirosawa, Wako, Saitama 351-0198, Japan.

Correspondence e-mail: hashi@postman.riken.go.jp

Received 14 November 2002
Accepted 12 March 2003

The process of the first-order solid-to-solid phase transition of 1-ethyl-3-(4-methylpentanoyl)urea (1) was observed by means of a detailed temperature-resolved single-crystal diffraction method, which resembles watching a series of stop-motion photographs. The transition consists of two elementary processes, one supramolecular and the other molecular. Crystal structures from before and after the phase transition are isostructural. The straight-ribbon-like one-dimensional hydrogen-bonding structure is formed and stacked to form a molecular layer. The geometry of the layer is retained during the phase transition. The relative position of the layer with its neighbours, on the other hand, changes gradually with increasing temperature. The change is accelerated at the temperature representing the start of the endotherm seen in the DSC curves of (1). The structural variation yields void space between the neighbouring layers. When the void space grows enough that the crystal is unstable, the 3-methylbutyl group on the last of the molecules turns into a disordered structure with drastic conformational changes to fill up the void space. The phase transition process is well supported with simple force-field calculations. A crystal of 1-(4-methylpentanoyl)-3-propylurea (2), which shows no solid-to-solid phase transitions, was also analysed by the same method for comparison.

1. Introduction

Phase transitions between polymorphs are very common in organic as well as inorganic crystals. The mechanisms of the transformations, however, are largely unknown despite the high importance in solid-state chemistry and material science (Dunitz & Bernstein, 1995). Diffraction methods are the most promising methods to elucidate the mechanism from a viewpoint of crystal and molecular structures. Powder diffraction has been widely used and has played an important role in the study of phase transitions in inorganic crystals. For organic crystals with low symmetries, however, crystal structure analysis utilizing powder diffraction data is generally difficult owing to the disadvantage of the number of data. Single-crystal diffraction, on the other hand, is suitable for analysing crystal structures in detail. Unfortunately, since phase transitions, especially first-order phase transitions, cause the collapse of the single crystal under study, the application of single-crystal diffraction has been almost restricted to high-order phase transitions.

Some single-crystal-to-single-crystal first-order phase transitions of organic crystals have been reported (Gafner, 1960, 1964; Kaftory *et al.*, 2001; Schmidt *et al.*, 1999; Steiner *et al.*, 1993; Zamir *et al.*, 1994). Low- and high-temperature phases

Table 1
Experimental details for (1).

Temperature (K)	98	298	328	348	350	352
Formula	$C_9H_{18}N_2O_2$	$C_9H_{18}N_2O_2$	$C_9H_{18}N_2O_2$	$C_9H_{18}N_2O_2$	$C_9H_{18}N_2O_2$	$C_9H_{18}N_2O_2$
Formula weight	186.25	186.25	186.25	186.25	186.25	186.25
Crystal system	Triclinic	Triclinic	Triclinic	Triclinic	Triclinic	Triclinic
Space group	$P\overline{1}$	$P\overline{1}$	$P\overline{1}$	$P\overline{1}$	$P\overline{1}$	$P\overline{1}$
a (Å)	8.704 (1)	8.8173 (5)	8.782 (2)	8.740 (2)	8.751 (2)	8.750 (2)
b (Å)	12.204 (3)	12.434 (1)	12.381 (2)	12.357 (2)	12.460 (2)	12.421 (1)
c (Å)	4.975 (1)	5.0963 (1)	5.111 (1)	5.147 (1)	5.1254 (9)	5.0998 (3)
α (°)	93.02 (1)	92.91 (1)	92.491 (8)	91.509 (8)	91.510 (5)	90.921 (8)
β (°)	90.616(7)	89.876(3)	90.164(9)	90.24(1)	90.273(9)	89.72(1)
γ (°)	90.32 (1)	90.15 (1)	89.589 (9)	89.53 (1)	89.642 (8)	89.71 (1)
V (Å^3)	527.6 (2)	558.00 (6)	555.2 (2)	555.7 (2)	558.7 (2)	554.2 (1)
Z	2	2	2	2	2	2
D_x (Mg m^{-3})	1.172	1.109	1.114	1.113	1.107	1.116
Crystal description						
Colour	Colourless	Colourless	Colourless	Colourless	Colourless	Colourless
Shape	Plate	Plate	Plate	Plate	Plate	Plate
Size (mm)	0.8 × 0.4 × 0.1	0.8 × 0.4 × 0.1	0.8 × 0.4 × 0.1	0.8 × 0.4 × 0.1	0.8 × 0.4 × 0.1	0.8 × 0.4 × 0.1
Radiation	Mo $K\alpha$	Mo $K\alpha$	Mo $K\alpha$	Mo $K\alpha$	Mo $K\alpha$	Mo $K\alpha$
μ (mm^{-1})	0.083	0.078	0.079	0.079	0.078	0.079
$2\theta_{max}$ (°)	55	55	55	55	55	55
Index ranges	$-10 \le h \le 11$	$-11 \le h \le 11$	$-11 \le h \le 11$	$-10 \le h \le 10$	$-11 \le h \le 11$	$-11 \le h \le 11$
	$-15 \le k \le 15$	$-16 \le k \le 16$	$-15 \le k \le 16$	$-15 \le k \le 15$	$-16 \le k \le 16$	$-16 \le k \le 16$
	$-6 \le l \le 6$	$-6 \le l \le 6$	$-6 \le l \le 6$	$-6 \le l \le 6$	$-6 \le l \le 6$	$-6 \le l \le 6$
Number of reflections						
Measured	6068	6494	7578	6205	6495	6495
Independent	2076	2292	2169	1939	2118	1968
Observed [$I > 2\sigma(I)$]	1992	2041	1728	1418	1790	1242
R_{int}	0.035	0.026	0.026	0.036	0.021	0.043
$R(F)$	0.045	0.057	0.060	0.082	0.120	0.109
$wR(F^2)$	0.126	0.164	0.148	0.231	0.241	0.312
S	1.10	1.09	1.08	1.06	1.34	2.28
$(\Delta/\sigma)_{max}$	≤ 0.00	≤ 0.00	≤ 0.00	≤ 0.00	≤ 0.00	≤ 0.00
$\Delta\rho_{min,max}$ (e Å^{-3})	−0.24, 0.27	−0.21, 0.16	−0.18, 0.17	−0.21, 0.27	−0.22, 0.20	−0.27, 0.25

Temperature (K)	354	356	358	360	362	364
Formula	$C_9H_{18}N_2O_2$	$C_9H_{18}N_2O_2$	$C_9H_{18}N_2O_2$	$C_9H_{18}N_2O_2$	$C_9H_{18}N_2O_2$	$C_9H_{18}N_2O_2$
Formula weight	186.25	186.25	186.25	186.25	186.25	186.25
Crystal system	Triclinic	Triclinic	Triclinic	Triclinic	Triclinic	Triclinic
Space group	$P\overline{1}$	$P\overline{1}$	$P\overline{1}$	$P\overline{1}$	$P\overline{1}$	$P\overline{1}$
a (Å)	8.7270 (4)	8.726 (3)	8.7438 (6)	8.756 (1)	8.670 (1)	8.711 (1)
b (Å)	12.601 (1)	12.460 (3)	12.527 (1)	12.579 (1)	12.5515 (9)	12.645 (1)
c (Å)	5.1459 (3)	5.138 (1)	5.1573 (4)	5.1472 (6)	5.1490 (5)	5.1787 (6)
α (°)	91.317 (9)	91.423 (6)	90.802 (6)	90.68 (1)	90.036 (7)	90.134 (7)
β (°)	90.33 (1)	90.14 (1)	90.388 (7)	90.707 (6)	91.078 (4)	90.557 (4)
γ (°)	89.001 (9)	89.30 (1)	89.224 (3)	89.216 (6)	88.834 (4)	88.953 (4)
V (Å^3)	565.65 (7)	558.5 (2)	564.77 (7)	566.8 (1)	560.11 (9)	570.3 (1)
Z	2	2	2	2	2	2
D_x (Mg m^{-3})	1.094	1.108	1.095	1.091	1.104	1.085
Crystal description						
Colour	Colourless	Colourless	Colourless	Colourless	Colourless	Colourless
Shape	Plate	Plate	Plate	Plate	Plate	Plate
Size (mm)	0.8 × 0.4 × 0.2	0.8 × 0.8 × 0.1	1.0 × 1.0 × 0.2	1.0 × 1.0 × 0.2	1.0 × 1.0 × 0.2	1.0 × 1.0 × 0.2
Radiation	Mo $K\alpha$	Mo $K\alpha$	Mo $K\alpha$	Mo $K\alpha$	Mo $K\alpha$	Mo $K\alpha$
μ (mm^{-1})	0.077	0.078	0.078	0.077	0.078	0.077
$2\theta_{max}$ (°)	55	55	55	55	55	55
Index ranges	$-11 \le h \le 11$	$-10 \le h \le 11$	$-11 \le h \le 11$	$-11 \le h \le 11$	$-11 \le h \le 11$	$-11 \le h \le 11$
	$-16 \le k \le 16$	$-15 \le k \le 15$	$-16 \le k \le 16$	$-16 \le k \le 16$	$-16 \le k \le 16$	$-16 \le k \le 16$
	$-6 \le l \le 6$	$-6 \le l \le 6$	$-6 \le l \le 6$	$-6 \le l \le 6$	$-6 \le l \le 6$	$-6 \le l \le 6$
Number of reflections						
Measured	6513	6409	6499	6442	6484	7726
Independent	2122	1713	2397	2389	2361	2503
Observed [$I > 2\sigma(I)$]	1551	1306	1516	1518	1478	1474
R_{int}	0.026	0.035	0.058	0.055	0.032	0.028
$R(F)$	0.118	0.079	0.103	0.100	0.094	0.091
$wR(F^2)$	0.259	0.220	0.280	0.277	0.288	0.259
S	1.31	1.08	1.83	1.04	1.06	1.05
$(\Delta/\sigma)_{max}$	≤ 0.00	≤ 0.00	≤ 0.00	≤ 0.00	≤ 0.00	≤ 0.00

Table 1 (continued)

$\Delta\rho_{min,\ max}$ (e Å^{-3})	−0.22, 0.22	−0.24, 0.23	−0.28, 0.36	−0.29, 0.31	−0.34, 0.37	−0.34, 0.33
Temperature (K)	366	368	370	372	374	
Formula	$C_9H_{18}N_2O_2$	$C_9H_{18}N_2O_2$	$C_9H_{18}N_2O_2$	$C_9H_{18}N_2O_2$	$C_9H_{18}N_2O_2$	
Formula weight	186.25	186.25	186.25	186.25	186.25	
Crystal system	Triclinic	Triclinic	Triclinic	Triclinic	Triclinic	
Space group	$P\overline{1}$	$P\overline{1}$	$P\overline{1}$	$P\overline{1}$	$P\overline{1}$	
a (Å)	8.716 (1)	8.6912 (5)	8.605 (2)	8.614 (2)	8.634 (1)	
b (Å)	12.6307 (7)	12.7757 (6)	12.855 (2)	12.994 (3)	13.178 (2)	
c (Å)	5.1642 (7)	5.1587 (1)	5.170 (1)	5.191 (1)	5.224 (2)	
α (°)	89.78 (1)	88.386 (2)	87.26 (2)	86.20 (1)	85.95 (1)	
β (°)	90.522 (6)	91.168 (6)	92.266 (9)	91.62 (1)	91.71 (2)	
γ (°)	88.757 (5)	88.463 (2)	88.060 (8)	88.099 (6)	88.03 (1)	
V (Å^3)	568.3 (1)	572.24 (4)	570.4 (2)	579.1 (2)	592.2 (2)	
Z	2	2	2	2	2	
D_x (Mg m^{-3})	1.088	1.081	1.084	1.068	1.044	
Crystal description						
Colour	Colourless	Colourless	Colourless	Colourless	Colourless	
Shape	Plate	Plate	Plate	Plate	Plate	
Size (mm)	1.0 × 1.0 × 0.2	1.0 × 1.0 × 0.2	1.0 × 1.0 × 0.2	1.0 × 1.0 × 0.6	1.0 × 1.0 × 0.6	
Radiation	Mo $K\alpha$	Mo $K\alpha$	Mo $K\alpha$	Mo $K\alpha$	Mo $K\alpha$	
μ (mm^{-1})	0.077	0.077	0.077	0.076	0.074	
$2\theta_{max}$ (°)	55	55	55	55	55	
Index ranges	$-11 \le h \le 11$	$-11 \le h \le 11$	$-11 \le h \le 11$	$-11 \le h \le 11$	$-11 \le h \le 11$	
	$-16 \le k \le 15$	$-16 \le k \le 16$	$-16 \le k \le 16$	$-16 \le k \le 16$	$-16 \le k \le 16$	
	$-6 \le l \le 6$	$-6 \le l \le 6$	$-6 \le l \le 6$	$-6 \le l \le 6$	$-6 \le l \le 6$	
Number of reflections						
Measured	6593	7417	9055	8178	8267	
Independent	2383	2283	2263	2312	1962	
Observed [$I > 2\sigma(I)$]	1377	1212	1016	1114	826	
R_{int}	0.033	0.021	0.031	0.040	0.041	
$R(F)$	0.100	0.099	0.116	0.124	0.152	
$wR(F^2)$	0.291	0.256	0.309	0.305	0.344	
S	1.05	1.07	1.07	1.75	1.85	
$(\Delta/\sigma)_{max}$	≤ 0.00	≤ 0.00	≤ 0.00	≤ 0.00	≤ 0.00	
$\Delta\rho_{min,\ max}$ (e Å^{-3})	−0.35, 0.32	−0.28, 0.24	−0.27, 0.28	−0.29, 0.39	−0.22, 0.22	

were analysed, but transition mechanisms were not fully represented in the literature. The structure analyses before and after the transition only provide static information and it is necessary to analyse the intermediate stages during the transition to elucidate the mechanism. This can be achieved by succeeding measurements at many temperature points during the transitions; we term such a method 'detailed temperature-resolved measurements'. The measurements will provide successive structural variations just going on the phase transition as a series of stop-motion photographs. Recently, direct observations of such dynamic processes have been reported for hydrogen transfer (Wilson, 2001) and high-order phase transitions (Katrusiak, 2001) by temperature-resolved single-crystal diffraction.

In a series of studies on the solid-to-solid phase transitions of 1-alkanoyl-3-alkylurea derivatives, we found that a crystal of 1-ethyl-3-(4-methylpentanoyl)urea (1) shows first-order solid-to-solid phase transitions at 363 K and the single crystalline state is retained during and after the phase transition. To elucidate the phase transition mechanism and its dynamic process we performed detailed temperature-resolved single-crystal diffraction measurements while passing through the transition for (1). A crystal of 1-(4-methylpentanoyl)-3-propylurea (2), which shows no solid-to-solid phase transi-

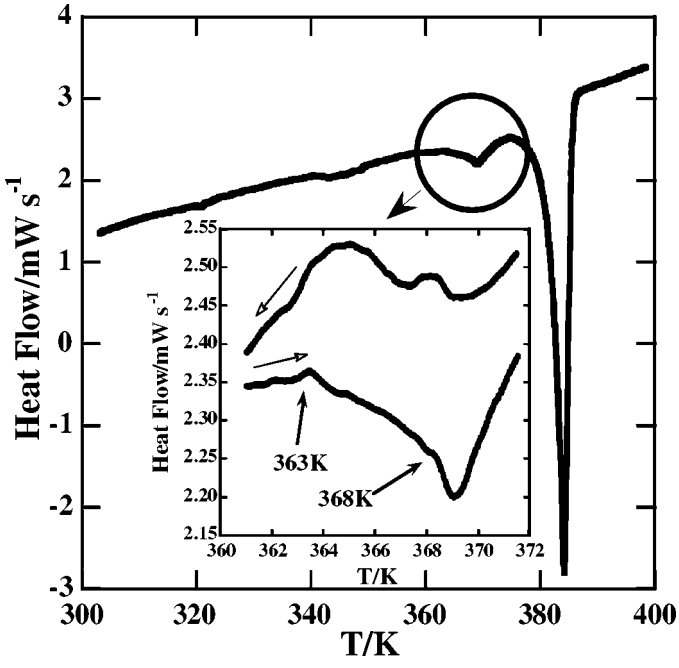

Figure 1
DSC curves of a crystal of (1).

tions, was also analysed by the same method for comparison. In this paper we report on the mechanism of the phase transition of (1) and the thermal behaviour of (2).

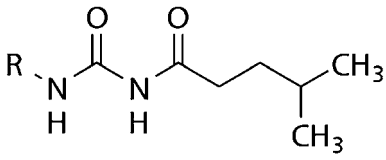

(1): R = Et
(2): R = Pr

2. Experimental

2.1. Preparation of samples

The acylurea derivatives (1) and (2) were prepared by adding 4-methylpentanoylisocyanate to the corresponding amines (ethylamine and *n*-propylamine) in acetonitrile at 273 K, as described previously (Endo *et al.*, 1982).

Single crystals of (1) and (2) were obtained from acetone–acetonitrile and acetonitrile solutions, respectively, by slow evaporation at room temperature.

2.2. Calorimetric measurement

Calorimetric experiments were performed on a differential scanning calorimeter, DSC8230D, Rigaku Ltd. All DSC measurements were carried out under an air atmosphere. Measurements were performed in the temperature range 303–403 K, in which heating–cooling cycles were repeated three times with a scan rate of 2 K min^{-1}. The calorimeter was calibrated with the melting point of (1).

2.3. Crystal structure analysis

The crystal data for (1) and (2) are summarized in Tables 1 and 2.[1] Specimens were coated with epoxy glue to prevent sublimation. Diffraction data were collected on an imaging-plate Weissenberg camera, Rigaku Raxis-Rapid, by an oscillation method using Mo $K\alpha$ radiation generated from a fine-focus sealed tube. Temperature was controlled to within $\pm$0.2 K by a gas-stream method using nitrogen gas.

For (1) data sets were collected at 98, 298 and 328 K, and at every 2 K in the range 348–374 K. The data collections were carried out at low temperature. Prior to data collection the specimen was kept at the required temperature for $\simeq$1 h in order to reach the specimen thermal equilibrium. Four crystals, which were changed at 356, 358 and 372 K, were used for the collection of a total of 17 data sets because the specimens sublimed during data collection. Bragg spots were not split in any data set. The structure of (1) at 98 K was solved by means of the *SIR*97 program (Altomare *et al.*, 1999) and refined by

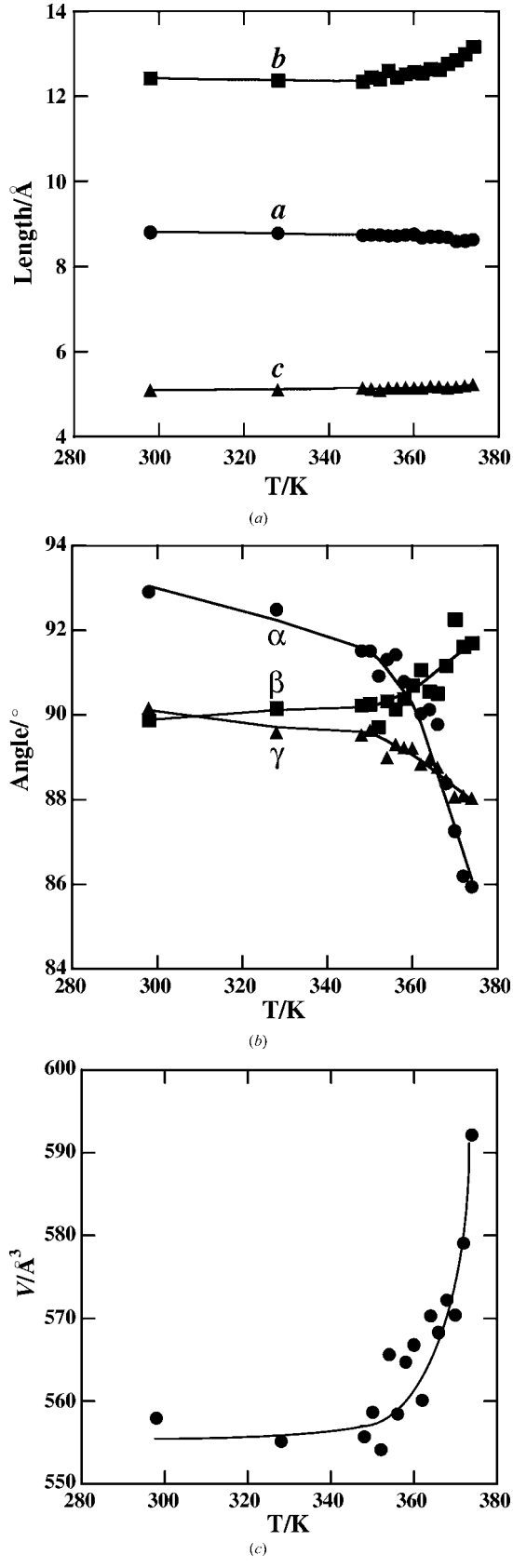

Figure 2
Variations in the cell constants of (1) with temperature: (*a*) *a*, *b* and *c* axes; (*b*) angles α, β and γ; (*c*) volume. Lines are drawn as guides to the eyes.

[1] Supplementary data for this paper are available from the IUCr electronic archives (Reference: LC0061). Services for accessing these data are described at the back of the journal.

Table 2
Experimental details for (2).

Temperature (K)	98	298	348
Formula	$C_{10}H_{20}N_2O_2$	$C_{10}H_{20}N_2O_2$	$C_{10}H_{20}N_2O_2$
M_r	200.28	200.28	200.28
Crystal system	Triclinic	Triclinic	Triclinic
Space group	$P\bar{1}$	$P\bar{1}$	$P\bar{1}$
a (Å)	9.544 (2)	9.547 (4)	9.405 (2)
b (Å)	13.205 (4)	13.688 (6)	13.360 (2)
c (Å)	4.846 (1)	5.117 (2)	5.1686 (8)
α (°)	92.03 (1)	90.90 (1)	93.61 (1)
β (°)	98.767 (9)	97.109 (8)	98.14 (1)
γ (°)	78.88 (2)	80.47 (2)	79.39 (1)
V (Å^3)	592.2 (3)	654.3 (4)	631.5 (2)
Z	2	2	2
D_x (Mg m^{-3})	1.123	1.017	1.053
Crystal description			
Colour	Colourless	Colourless	Colourless
Shape	Plate	Plate	Plate
Size (mm)	0.5 × 0.3 × 0.1	0.5 × 0.3 × 0.1	0.5 × 0.3 × 0.1
Radiation	Mo $K\alpha$	Mo $K\alpha$	Mo $K\alpha$
μ (mm^{-1})	0.078	0.071	0.073
$2\theta_{max}$ (°)	55	55	55
Index ranges (h, k, l)	$-11 \le h \le 12$ $-16 \le k \le 17$ $-6 \le l \le 6$	$-12 \le h \le 12$ $-17 \le k \le 17$ $-6 \le l \le 6$	$-10 \le h \le 12$ $-13 \le k \le 16$ $-6 \le l \le 6$
Number of reflections			
Measured	6949	10 255	10 152
Independent	2162	2485	1576
Observed	1775	1178	861
Criterion for observed reflections	$I > 2\sigma(I)$	$I > 2\sigma(I)$	$I > 2\sigma(I)$
R_{int}	0.051	0.071	0.078
$R(F)$	0.062	0.117	0.140
$wR(F^2)$	0.153	0.313	0.340
S	1.06	1.97	2.05
$(\Delta/\sigma)_{max}$	≤0.00	≤0.00	≤0.00
$\Delta\rho_{min,\ max}$ (e Å^{-3})	−0.25, 0.31	−0.32, 0.34	−0.18, 0.23

the full-matrix least-squares procedures with the *SHELXL*97 program (Sheldrick, 1997). The refined structure at each temperature was used in turn as the initial model for the refinement of the structure at succeeding temperatures.

The diffraction data for (2) were collected at 98, 298 and 348 K. The structure at 98 K was solved and refined, as was that of (1) at 98 K. Structures at successive temperatures were also refined in the same manner as for (1). For all data sets, because of the poor crystallinity of the specimens and high measuring temperature, the numbers of high-angle data were small but the distributions of observed reflections were random in an independent sphere.

2.4. Force-field calculation

Force-field calculations were performed for all the analysed structures of (1) with the program *Cerius*2 (Molecular Simulations Inc., 2000) using the UNIVERSAL force field (Castonguay & Rappe, 1992; Rappe *et al.*, 1992; Rappe & Colwell, 1993). Intermolecular energies were calculated as the energies among the original molecule, (x, y, z), and the three molecules in the neighbouring layer, $(1-x, 2-y, 1-z)$, $(x, 1+y, z)$ and $(1-x, 2-y, -z)$. The positions of the H atoms were optimized before the calculations. To calculate the major–major contact, molecular structures at each temperature were used for the low-temperature phase and only the structures of the major parts were used for the high-temperature phase. To calculate the minor–major contact, the 3-methylbutyl group of the original molecule was set to take the same torsion angles as the minor conformer at 368 K for the low-temperature phase, and only the original molecule was set to have the minor conformer at each temperature for the high-temperature phase.

3. Results and discussion

3.1. Calorimetric investigation

Differential scanning calorimetry (DSC) curves of a powdered sample of (1) are shown in Fig. 1. The thermal behaviour of (1) was reversible in the measured temperature range. A sharp endothermic peak of the melting point

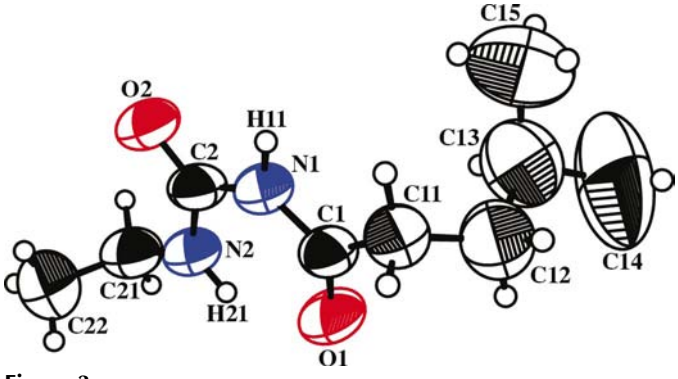

Figure 3
Molecular structure of (1) at 366 K.

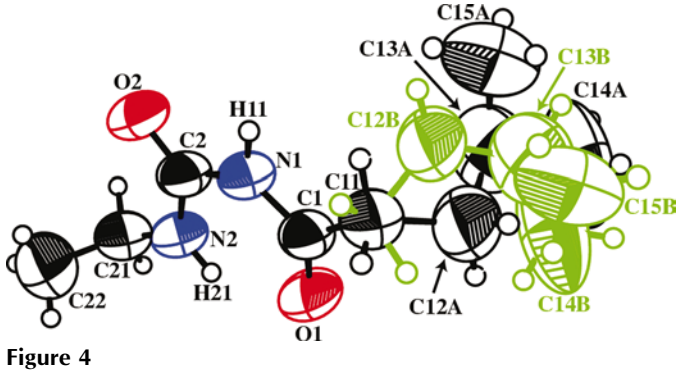

Figure 4
Molecular structure of (1) at 368 K. The minor part of the disordered 3-methylbutyl group is in green.

Table 3
Selected torsion angles (°).

T (K)	O1—C1—C11—C12 (°)	C1—C11—C12—C13 (°)	C11—C12—C13—C14 (°)	C11—C12—C13—C15 (°)
For (1)				
98	58.3 (2)	65.9 (1)	−175.1 (1)	62.5 (2)
298	56.7 (2)	66.0 (2)	−174.7 (2)	62.9 (2)
328	55.6 (3)	65.7 (3)	−174.8 (3)	63.1 (4)
348	55.3 (4)	65.7 (5)	−175.0 (4)	64.8 (6)
350	55.4 (6)	66.8 (6)	−175.6 (5)	64.3 (7)
352	55.9 (5)	66.3 (6)	−174.6 (6)	63.9 (8)
354	54.2 (6)	66.9 (6)	−175.8 (6)	64.0 (8)
356	55.1 (5)	66.6 (5)	−175.2 (5)	63.5 (6)
358	54.6 (4)	66.9 (5)	−175.7 (5)	63.1 (6)
360	54.4 (5)	67.5 (6)	−175.5 (6)	63.5 (7)
362	54.3 (5)	67.6 (6)	−175.0 (6)	63.7 (8)
364	53.8 (5)	68.3 (6)	−174.8 (6)	64.2 (8)
366	53.9 (6)	69.0 (7)	−174.6 (7)	64 (1)
368†	52.5 (6)	70.6 (7)	−176.5 (7)	66.5 (9)
	110 (1)	−132 (2)	68 (3)	−55 (3)
370†	50.8 (8)	72 (1)	−178 (1)	68 (1)
	107 (1)	−135 (2)	76 (3)	−47 (3)
372†	49.9 (5)	78.5 (7)	−176.3 (9)	65 (1)
	100.4 (7)	−145 (1)	89 (2)	−33 (2)
374†	51.0 (7)	81 (1)	−177 (1)	60 (2)
	106.2 (9)	−148 (1)	81 (2)	−41 (2)
For (2)				
98	94.6 (3)	−173.8 (2)	174.3 (2)	−61.3 (3)
298	89.0 (5)	−172.6 (4)	173.6 (6)	−62.5 (8)
348	89.5 (9)	−169.7 (8)	175 (1)	−70 (1)

† Values for the major and minor parts are listed on the upper and lower lines, respectively, in each temperature line.

appeared in the 375–387 K region with a peak at 384 K. The absorption was 17.3 kJ mol^{-1}. A very broad and shallow endothermic peak appeared just below the melting point. Gentle absorption started at 363 K and the slope became steep at 368 K. The absorption continued until melting began (375 K) passing through the peak at 369 K. The absorption was 1.1 kJ mol^{-1}. This absorption implies the occurrence of a first-order phase transition and that the transition consists of two elementary processes. The DSC curves were well reproduced three times by repeating the heating–cooling cycles.

3.2. Temperature dependence of cell constant in (1)

Fig. 2 shows the temperature dependence of cell constants in (1). All changes of the cell constants are continuous. The *b* axis is significantly elongated as temperature increases. The change in the *b* axis is almost linear until 362 or 364 K, as with other axes. The variation rate of the *b* axis becomes sharp above 364 K. This point corresponds to the start of thermal absorption at 363 K, but not to the inflection point of the DSC curvature at 368 K. The temperature dependences of the angles and the volume of the unit cell show large dispersions but show inflection points near 360 K.

3.3. Molecular structure of (1) at low-temperature phase

The molecular structures of (1) at 366 K are shown in Fig. 3. The structure is essentially the same as at lower temperatures. The carbonylurea moiety is planar and is bonded to 3-methylbutyl and ethyl groups with sc^+ and sc^- conformations, respectively. As a consequence of the conformations, the 3-methylbutyl and ethyl groups protrude from opposite faces of the carbonylurea plane from each other. The internal conformation of the 3-methylbutyl group around the C1—C11 and C11—C12 bonds varies little by little with temperature, as listed in Table 3.

3.4. Molecular structure of (1) at high-temperature phase

Above 368 K, which corresponds to the inflection point of an endothermic peak for the phase transition on the DSC curves, the 3-methylbutyl group became disordered over two sites with drastic conformational change, as shown in Fig. 4. Nevertheless, the molecules are packed in a crystal environment. Other moieties of the molecule have almost the same structure as that of the low-temperature phase. The conformation of the 3-methylbutyl group with a higher occupancy factor, the major conformation, is almost the same as that of the low-temperature phase, while the minor conformation is different. The corresponding torsion angles are listed in Table 3. The conformational change, particularly around the C1—C11 and C11—C12 bonds, makes the molecular length extend along the longest molecular axis, as illustrated in Fig. 5. The occupancy of the minor part is gradually increased with a temperature increase from

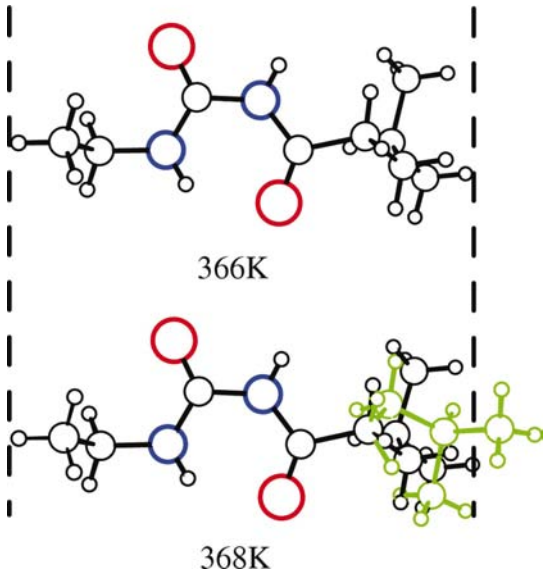

Figure 5
Comparison of the molecular length of (1). The minor part of the disordered moiety is in green.

Table 4
Hydrogen-bonding geometry (Å, °).

T (K)	N1···O2 (Å)	N1—H11···O2 (°)	N2···O1 (Å)	N2—H21···O1 (°)
For (1)				
98	2.822 (1)	179 (2)	2.978 (2)	137 (2)
298	2.853 (2)	177	3.057 (2)	137
328	2.858 (2)	177 (2)	3.067 (2)	136 (2)
348	2.859 (3)	177	3.069 (3)	137
350	2.853 (4)	178	3.070 (4)	137
352	2.840 (4)	179	3.047 (4)	137
354	2.850 (5)	177	3.073 (4)	137
356	2.844 (4)	177	3.073 (4)	137
358	2.861 (3)	178	3.085 (3)	137
360	2.867 (3)	178	3.092 (4)	137
362	2.866 (3)	178	3.077 (4)	137
364	2.860 (3)	178	3.083 (3)	137
366	2.855 (4)	178	3.085 (4)	137
368	2.863 (4)	178	3.098 (4)	137
370	2.870 (5)	178	3.107 (5)	138
372	2.855 (4)	178	3.100 (3)	138
374	2.862 (5)	178	3.107 (5)	139
For (2)				
98	2.820 (3)	178 (3)	2.959 (3)	137 (3)
298	2.873 (4)	174	3.092 (4)	138
348	2.815 (7)	175	3.043 (8)	138

0.138 (6), at 368 K, to 0.235 (6), at 374 K; the change is complete at 372 K. The occupancies for the major and minor parts are 0.765 (6) and 0.235 (6), respectively, at the final stage of the phase transition, 374 K.

3.5. Crystal structures of (1) at both phases

Crystal structures of (1) at the low- and high-temperature phases are compared in Figs. 6 and 7. The crystal structures of the two phases are isostructural, or the packing motif, Z value and space group remain unchanged throughout the transition. The carbonylurea moieties are attached *via* hydrogen bonds to form straight-ribbon structures along the [$\bar{1}$01] direction. The geometries of the hydrogen bonds are summarized in Table 4. The ribbons are stacked along the [121] direction to form layers, which are parallel to the (010) face. The carbonyl groups contact each other betwen the ribbons in an anti-parallel manner with comparable distances to the sum of the van der Waals radii, 3.22 Å (Bondi, 1964). Owing to the contacts, the ribbons in the layer are strongly bound by the dipole–dipole interaction. The distances between the carbonyl groups show low temperature dependence and the corresponding distances are listed in Table 5.

The layers align along the b axis. The alkyl groups on both terminals of the carbonylurea moiety are packed between the layers with some short contacts, with distances comparable to the corresponding van der Waals contacts. Comparing the strength of the packing forces within and between the layers qualitatively, the latter is weaker than the former. This also accounts for the considerable thermal expansion of the b axis.

3.6. Variation of crystal structure of (1) with temperature

Fig. 8 shows the temperature dependence of intermolecular contacts and of the packing geometry of (1). No significant changes are observed in the interplanar distance between the

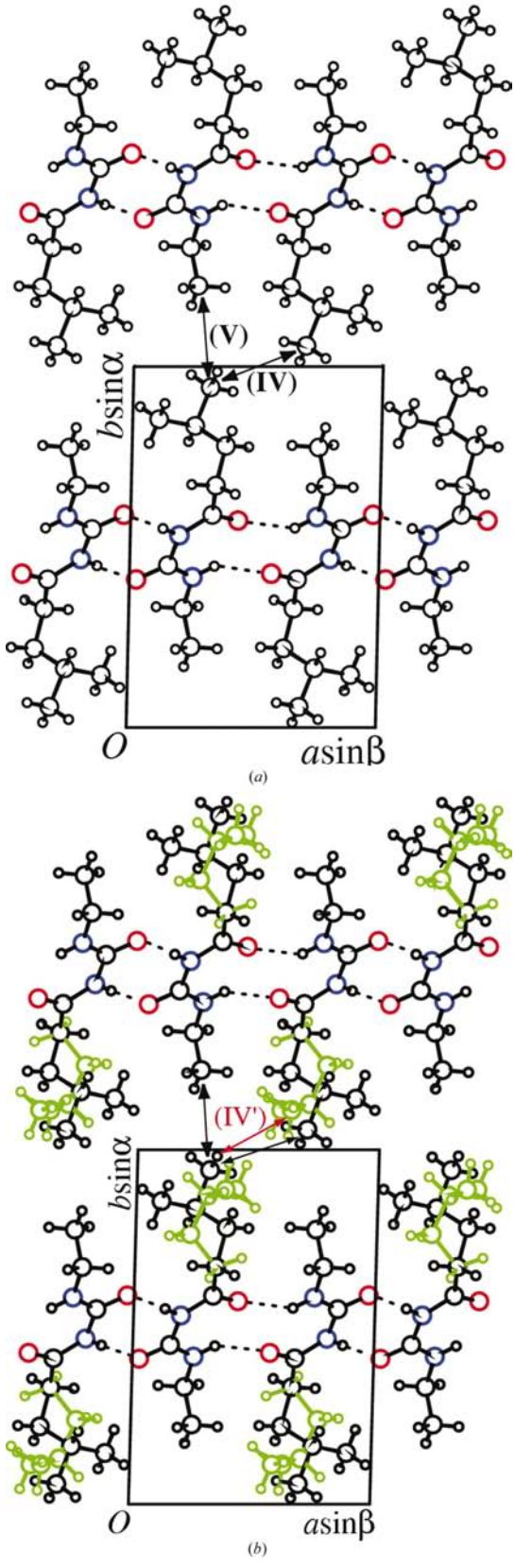

Figure 6
Crystal structures of (1) viewed along the c axis at (*a*) 366 and (*b*) 368 K. The minor parts of the disordered 3-methylbutyl groups are in green. The definitions of the intermolecular contacts highlighted in the figure are given in *Appendix A*.

Table 5
Intermolecular contacts of carbonyl groups of (1).

T (K)	O1···C1 (Å)	O2···C2 (Å)
98	3.371 (2)	3.159 (2)
298	3.530 (2)	3.301 (2)
328	3.517 (3)	3.302 (3)
348	3.521 (4)	3.306 (4)
350	3.528 (5)	3.318 (5)
352	3.541 (5)	3.312 (5)
354	3.536 (5)	3.328 (5)
356	3.543 (4)	3.322 (4)
358	3.537 (4)	3.325 (4)
360	3.534 (4)	3.321 (4)
362	3.512 (4)	3.308 (4)
364	3.551 (4)	3.346 (4)
366	3.557 (5)	3.339 (5)
368	3.528 (5)	3.333 (5)
370	3.490 (6)	3.302 (6)
372	3.549 (5)	3.364 (5)
374	3.582 (7)	3.393 (6)

stacked plates, (I). In addition, the variations are small for the geometries of the hydrogen bonds and the intermolecular distance of the carbonyl groups between the ribbons. The temperature dependence of the structure within the layer is consequently small. Variation related to the thermal expansion of the *b* axis is found for the distance between layers (II), as mentioned previously.

Variations in the distances (II) and (III) make the distance between the 3-methylbutyl groups (IV) longer along the longest molecular axis. Despite the spreading of the interlayer distance (II), on the other hand, the distance between the ethyl and 3-methylbutyl groups (V) is retained by the sliding motions of the layers.

Three types of contact between the 3-methylbutyl groups [symmetry codes (x, y, z) and $(1-x, 2-y, 1-z)$] are considered in the high-temperature phase, *i.e.* major–major, minor–major and minor–minor contacts (*Appendix B*). Only the major–major and minor–major contacts, however, are taken into account in the crystal, because steric repulsion is very high if the minor structures are in contact. The ratio[2] of the major–major and minor–major contacts in the crystal is calculated for 53 and 47%, respectively, at 374 K from the occupancies. This means that the major–major and the minor–major contacts between the 3-methylbutyl groups contribute equally to crystal packing in the final stages of the phase transition.

3.7. Mechanism of phase transition of (1)

Changes in the intermolecular geometries of (I)–(V) clarify the mechanism of the phase transition (Fig. 9). The layers glide along the [101] direction in order to keep contact between the ethyl and 3-methybutyl groups with increasing temperature, namely the supramolecular process. The supramolecular process, however, brings about a lack of contact of the 3-

[2] When the occupancies of the major and minor parts are *a* and *b*, respectively, and there are only the major–major and minor–minor contacts, the ratio for two kinds of contacts in the crystal is calculated as $(a-0.5)/0.5$ and $b/0.5$ for the major–major and minor–major contacts, respectively.

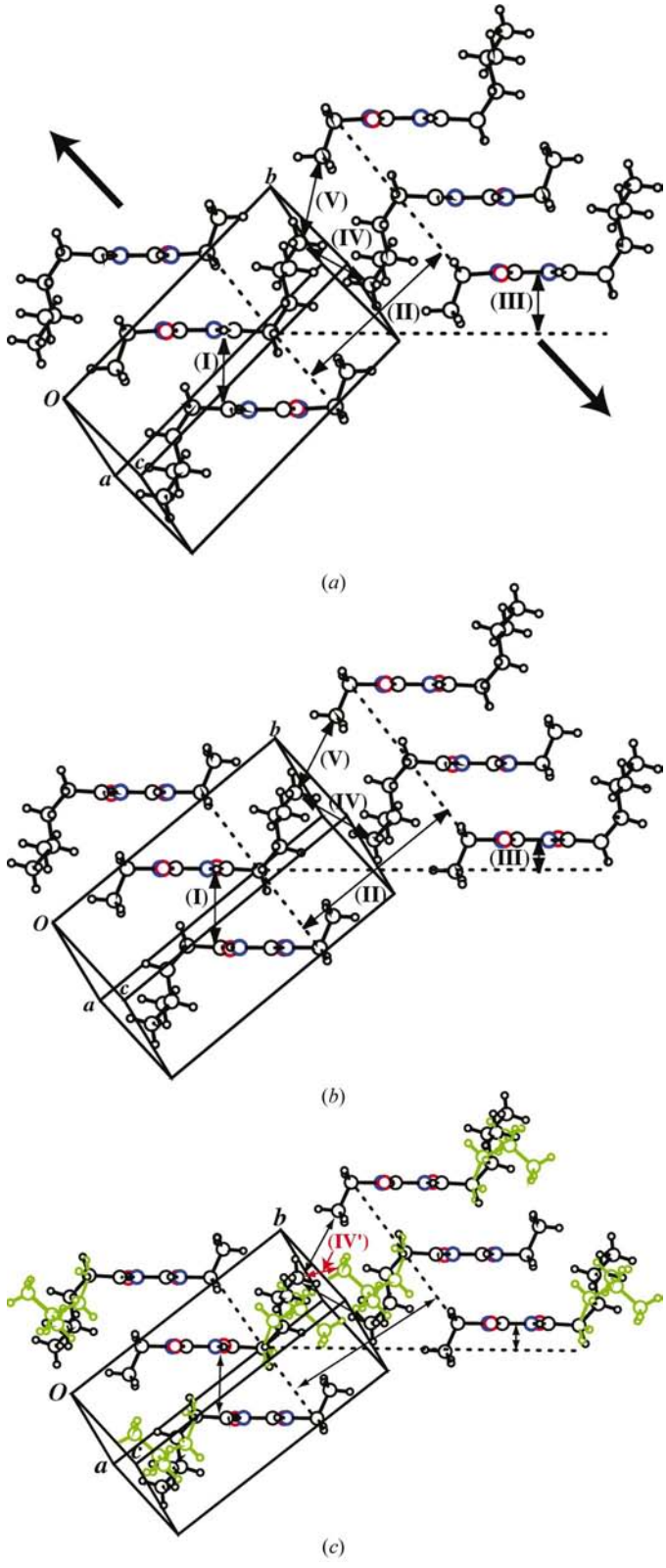

Figure 7
Crystal structures of (1) viewed along the hydrogen-bonding ribbons at (*a*) 98, (*b*) 366 and (*c*) 368 K. The minor part of the disordered 3-methylbutyl group is in green. The definitions of the intermolecular contacts highlighted in the figure are given in *Appendix A*. Thick arrows in (*a*) indicate the direction of the supramolecular motions of the molecular layers.

methylbutyl groups faced between the neighbouring layers. Since the process occurs at all temperatures, the lack of the contact is accumulated as void space even at the low-temperaure phase with increasing temperature, and the supramolecular process is enhanced when the temperature reaches about 360 K. The temperature increases and the void space becomes large enough that the crystal becomes unstable; some fractions of the 3-methylbutyl groups in the crystal are then disordered with drastic conformational change to fill up the void space, namely a molecular process, and thereby the crystal is transformed into the high-temperature phase.

The transition mechanism also explains the relationship between the profile of the DSC (differential scanning calorimetry) curve and the phase transition process. The starting point of absorption of heat for the phase transition, 363 K, corresponds to the point where the supramolecular process is enhanced and the inflection point on the DSC curve at 368 K corresponds to the start of the molecular process.

3.8. Energetic consideration of the phase transition

Force-field calculations were performed to ensure the transition mechanism is correct energetically. Four molecules were considered for the calculations: the original molecule (x, y, z) and symmetry-related molecules contacting with the 3-methylbutyl group of the original molecule by the 3-methylbutyl group $(1-x,\ 2-y,\ 1-z)$ and ethyl groups $(x, 1+y, z)$ and $(1-x, 2-y, -z)$. Van der Waals and electrostatic energies, which were calculated for the structures of each temperature, and their sums are illustrated in Figs. 10 and 11 for the major–major and minor–major contacts, respectively. The van der Waals energy of the major–major contact increases gradually with increasing temperature and the variation becomes steep above 362 K. The change is due to the variation of the intermolecular distance between the 3-methylbutyl groups. The electrostatic energy, on the other hand, decreases rapidly above 364 K. This brings about a decrease in the total intermolecular energy. Contrary to this, the total intermolecular energy for the minor–major contact decreases drastically with temperature and becomes negative between 366 and 368 K. The energies at these temperatures are comparable to those of the major–major contact. The molecular energies are calculated as −316 and −330 kJ mol^{-1} for the major and minor conformers, respectively, at 368 K. The transformation from the major conformer to the minor conformer, therefore, occurs spontaneously above 368 K. The

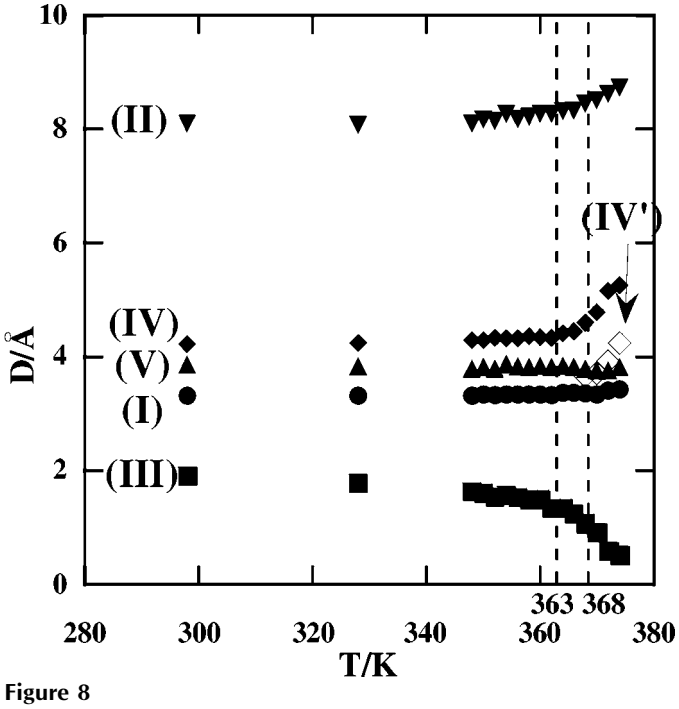

Figure 8
Temperature dependence of the intermolecular contacts and packing geometries in a crystal of (1). Lines are drawn as guides to the eyes.

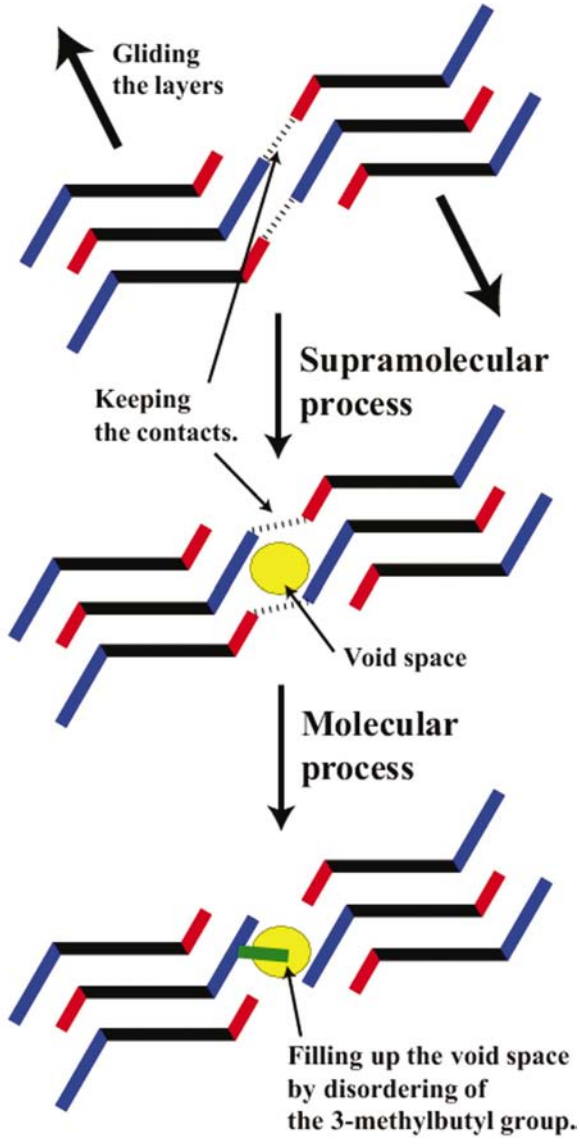

Figure 9
Schematic representation of the supra and molecular processes. The carbonylurea, 3-methylbutyl and ethyl groups are shown in black, blue and red, respectively. In the bottom figure, the major and minor conformers of the disordered 3-methylbutyl group are shown in blue and green, respectively.

difference in molecular energies could be a driving force for the consequent conformational change of the 3-methylbutyl group.

3.9. Crystal and molecular structures, and thermal behaviour of (2)

Figs. 12 and 13 show the molecular and crystal structures of (2), respectively, which shows no first-order solid-to-solid phase transition in the range 98–381 K (melting point). The carbonylurea moiety is planar and is bonded to 3-methylbutyl and propyl groups with ac^{+} and ac^{-} conformations, respectively, at 98 K. The internal conformation of the 3-methylbutyl group resembles that of the minor part in crystals of (1) at the high-temperature phase rather than those in the major part and the low-temperature phase. The similar internal conformation leads to a similar length of the 3-methylbutyl moiety to that of (1) along the longest molecular axis.

The packing motif of (2) is very similar to that of (1), but the crystals are not isostructural. The carbonylurea moiety is hydrogen bonded to the molecules related by crystallographic inversion centres to form a straight-ribbon structure along the [101] direction. The ribbons are stacked along the [$\bar{1}$21] direction to form a layer parallel to the (010) face. The stacking manner, however, is different from that of (1), in which short anti-parallel contacts of carbonyl groups are not found. The alkyl groups on both terminals of the carbonylurea moiety are packed between the layers. Unfortunately, since the sublimation of the specimen was pronounced during data collection, data sets were not obtained near the melting point.

Despite the absence of data near the melting point, the sliding of the layers, corresponding to the supramolecular process of the phase transition of (1), was observed accompanied with the thermal expansion of the crystal, as observed in (1) (Fig. 14). The displacement of the layer by the sliding motion becomes larger and interlayer contacts become weaker with temperature. Accordingly, the crystal will melt without a solid-to-solid phase transition. Since the length of the 3-methylbutyl group is similar to the minor structure of (1) along the longest molecular axis, the conformational change of the 3-methylbutyl group could not fill up the resultant void space forming along the longest molecular axis.

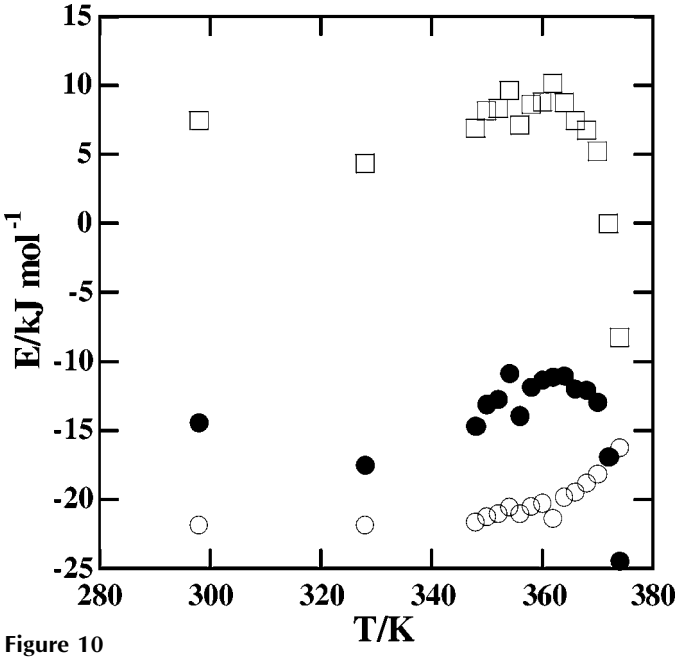

Figure 10
Variations in the intermolecular energy of the major–major contact in crystals of (1). Open circles and squares, and filled circles indicate intermolecular van der Waals, electrostatic and total energies, respectively.

4. Conclusions

The mechanism of the solid-to-solid first-order phase transition of (1) is clarified by analysing the structures of intermediate stages of the transition by detailed temperature-

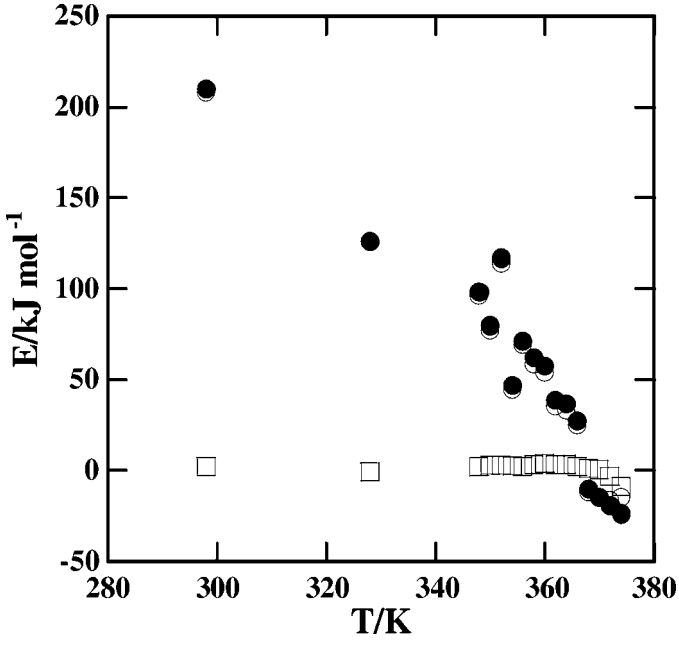

Figure 11
Variations in the intermolecular energy of the minor–major contact in crystals of (1). Open circles and squares, and filled circles indicate intermolecular van der Waals, electrostatic and total energies, respectively.

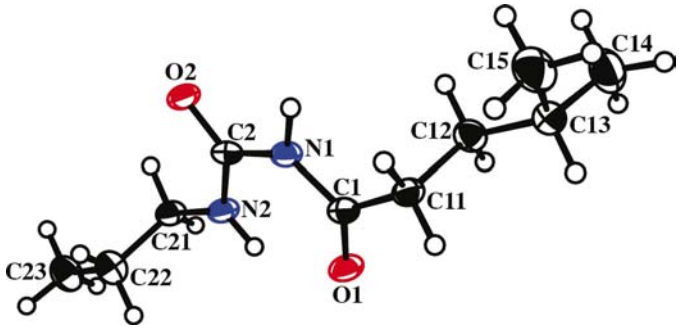

Figure 12
Molecular structure of (2) at 98 K.

resolved measurements. The transition proceeds with two elementary processes, *i.e.* supramolecular and molecular processes, as follows:

(i) the *b* axis is elongated;

(ii) the molecular layers composed of the stacked hydrogen-bonded straight-ribbons glide along the interface between them to keep contact of facing ethyl and 3-methylbutyl groups between the neighbouring layers (supramolecular process);

(iii) the distance between the 3-methylbutyl groups is increased and void space is developed between them;

(iv) the void space becomes large enough that the crystal is unstable, then some fractions of 3-methylbutyl groups change conformations to fill up some resultant vacancies in the crystal (molecular process).

The mechanism explains well the relationship between the profile of the DSC curve and variations of the crystal and molecular structures. The starting point of absorption of heat for the phase transition, 363 K, corresponds to the point at which the gliding of the layers is enhanced and the inflection point on the DSC curve, 368 K, corresponds to the start of disorder in the 3-methylbutyl group. The minor conformation caused by the disorder is more stable than that of the major structure.

A crystal of (2) with very similar crystal structure does not show a first-order phase transition as in (1). The variation in the relative position of the molecular layers is also observed accompanied with the thermal expansion of the crystal. Since alkyl groups on both terminals of the carbonylurea moiety have similar internal conformations to that of the minor part of the disordered 3-methylbutyl group in the crystal of (1) at high-temperature phase, the resultant void space generated by supramolecular motion of the molecular layer is no longer filled up by the disorder of the 3-methylbutyl group, as in a crystal of (1).

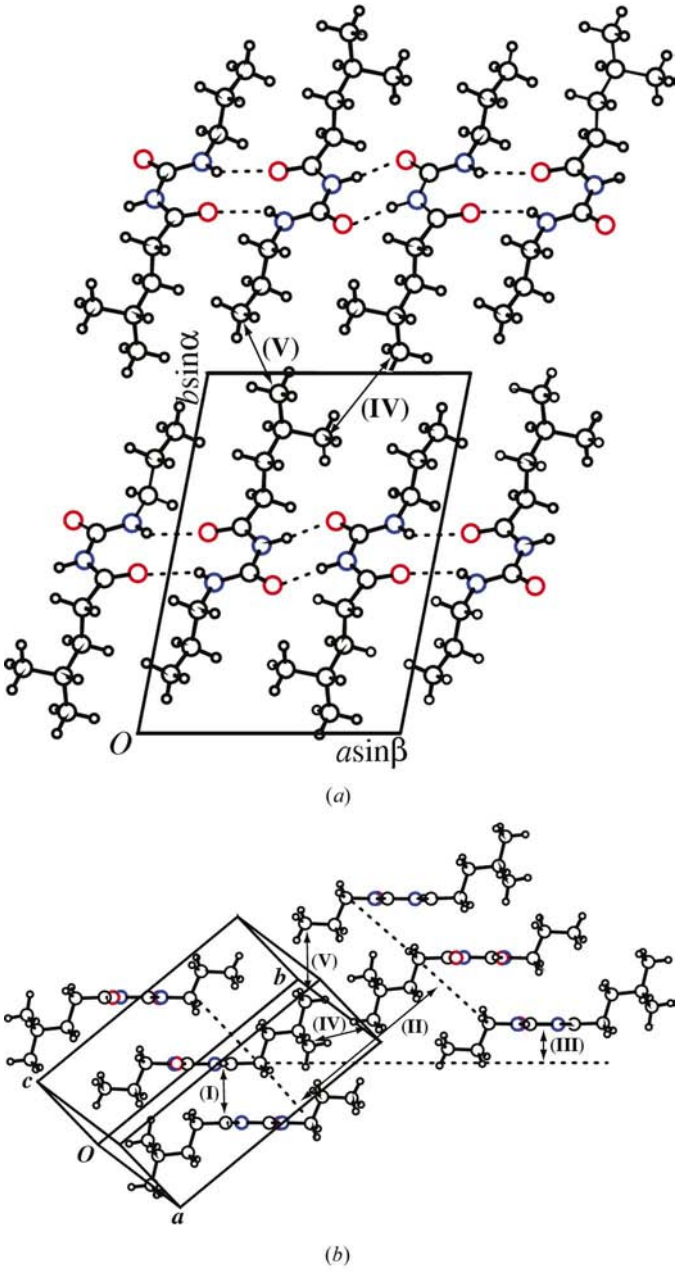

Figure 13
Crystal structures of (2) at 98 K: (*a*) viewed along the *c* axis and (*b*) viewed along the hydrogen-bonding ribbons. The definitions of the intermolecular contacts highlighted in the figure are given in *Appendix A*.

APPENDIX *A*
Definitions of the intermolecular distances

Definitions of the intermolecular distances of (I), (II), (III), (IV) and (V) of (1) are as follows:

(I) Distance between the following two least-squares planes defined by (O1 O2 N1 N2 C1 C2)—(O1 O2 N1 N2 C1 C2)^{i}—(O1 O2 N1 N2 C1 C2)^{ii}—(O1 O2 N1 N2 C1 C2)^{iii} and (O1 O2 N1 N2 C1 C2)^{iv}—(O1 O2 N1 N2 C1 C2)^{v}—(O1 O2 N1 N2 C1 C2)^{vi}—(O1 O2 N1 N2 C1 C2)^{vii}.

(II) Distance between the neighbouring layers defined as the least-squares planes composed from C atoms on the C- and N-terminals of carbonylurea moieties in each layer; C21^{i}—C11—C21^{ii}—C11^{iii}—C11^{iv}—C21^{v}—C11^{vi}—C21^{viii} and C11^{ix}—C21^{x}—C11^{xi}—C21^{xii}—C21^{xiii}—C11^{xiv}—C21^{xv}—C11^{xvi}.

(III) Relative distance between the least-squares planes of straight ribbons in the neighbouring layers defined by (O1 O2 N1 N2 C1 C2)—(O1 O2 N1 N2 C1 C2)^{i}—(O1 O2 N1 N2 C1 C2)^{ii}—(O1 O2 N1 N2 C1 C2)^{iii} and (O1 O2 N1 N2 C1 C2)^{x}—(O1 O2 N1 N2 C1 C2)^{xi}—(O1 O2 N1 N2 C1 C2)^{xii}—(O1 O2 N1 N2 C1 C2)^{xvii}.

(IV) Distance between C atoms of the methyl groups in contacted 3-methylbutyl groups, C14$\cdots$C14^{xviii} and C14$\cdots$C14*A*^{xviii} for the low- and high-temperature phases, respectively.

(IV′) Distance between C atoms of the methyl groups in contacted 3-methyl butyl groups, C14*A*$\cdots$C15*B* ^{xviii} for the high-temperature phase.

(V) Distance between C atoms of the methyl groups in ethyl and 3-methylbutyl groups, C22$\cdots$C14^{xix} and C22$\cdots$C14A^{xix} for the low- and high-temperature phases, respectively.

Symmetry codes: (i) $-x, 1-y, 1-z$; (ii) $1-x, 1-y, -z$; (iii) $1+x, y, z-1$; (iv) $x, y, 1+z$; (v) $1-x, 1-y, 1-z$; (vi) $1+x, y, z$; (vii) $-x, 1-y, 2-z$; (viii) $2-x, 1-y, -z$; (ix) $1-x, 2-y, 2-z$; (x) $1+x, 1+y, 1+z$; (xi) $2-x, 2-y, 1-z$; (xii) $2+x, 1+y, z$; (xiii) $1+x, 1+y, 2+z$; (xiv) $2-x, 2-y, 2-z$; (xv) $2+x, 1+y, 1+z$; (xvi) $3-x, 2-y, 1-z$; (xvii) $1-x, 2-y, 2-z$; (xviii) $1-x, 2-y, 1-z$; (xix) $x, 1+y, z$; (xx) $-x, 1-y, -z$.

Definitions of the intermolecular distances of (I), (II), (III), (IV) and (V) of (2) are as follows:

(I) Distance between the following two least-squares planes defined by (O1 O2 N1 N2 C1 C2)—(O1 O2 N1 N2 C1 C2)^{i}—(O1 O2 N1 N2 C1 C2)^{ii}—(O1 O2 N1 N2 C1 C2)^{iii} and (O1 O2 N1 N2 C1 C2)^{iv}—(O1 O2 N1 N2 C1 C2)^{v}—(O1 O2 N1 N2 C1 C2)^{vi}—(O1 O2 N1 N2 C1 C2)^{vii}.

(II) Distance between the neighbouring layers defined as the least-squares planes composed of C atoms on the C and N terminals of the carbonylurea moieties in each layer; C21^{i}—C11—C21^{iii}—C11^{ii}—C11^{iv}—C21^{v}—C11^{vi}—C21^{vii} and C11^{viii}—C21^{ix}—C11^{x}—C21^{xi}—C21^{xii}—C11^{xiii}—C21^{xiv}—C11^{xv}.

(III) Relative distance between the least-squares planes of straight ribbons in the neighbouring layers defined by (O1 O2 N1 N2 C1 C2)—(O1 O2 N1 N2 C1 C2)^{i}—(O1 O2 N1 N2 C1 C2)^{ii}—(O1 O2 N1 N2 C1 C2)^{iii} and (O1 O2 N1 N2 C1 C2)^{viii}—(O1 O2 N1 N2 C1 C2)^{ix}—(O1 O2 N1 N2 C1 C2)^{x}—(O1 O2 N1 N2 C1 C2)^{xi}.

(IV) Distance between C atoms of the methyl groups in contacted 3-methylbutyl groups C15$\cdots$C14^{xiii}.

(V) Distance between C atoms of the methyl groups in 3-methylbutyl and propyl groups, C14$\cdots$C23^{xvi}.

Symmetry codes: (i) $1-x, 1-y, 1-z$; (ii) $1+x, y, 1+z$; (iii) $-x, 1-y, -z$; (iv) $x, y, z-1$; (v) $1-x, 1-y, -z$; (vi) $1+x, y, z$; (vii) $2-x, 1-y, 1-z$; (viii) $1-x, 2-y, -1-z$; (ix) $1+x, 1+y, z-1$; (x) $2-x, 2-y, -z$; (xi) $2+x, 1+y, z$; (xii) $x, 1+y, z-1$; (xiii) $1-x, 2-y, -z$; (xiv) $1+x, 1+y, z$; (xv) $2-x, 2-y, 1-z$; (xvi) $x, 1+y, z$.

APPENDIX *B*
Definition of terms of major–major and minor–major contacts

The major–major contact is defined as the contact of the 3-methylbutyl groups in the major orientation between neighbouring layers at the high-temperature phase. Minor–major and minor–minor contacts are analogues of the major–major contact; minor–major and minor–minor contacts are defined as contacts between minor and major conformers, and between minor and minor conformers, respectively, at the high-temperature phase.

This work was partly supported by a Grant-in-Aid for Scientific Research (No. 12640490) from the Ministry of Education, Science, Sports and Culture of the Japanese Government.

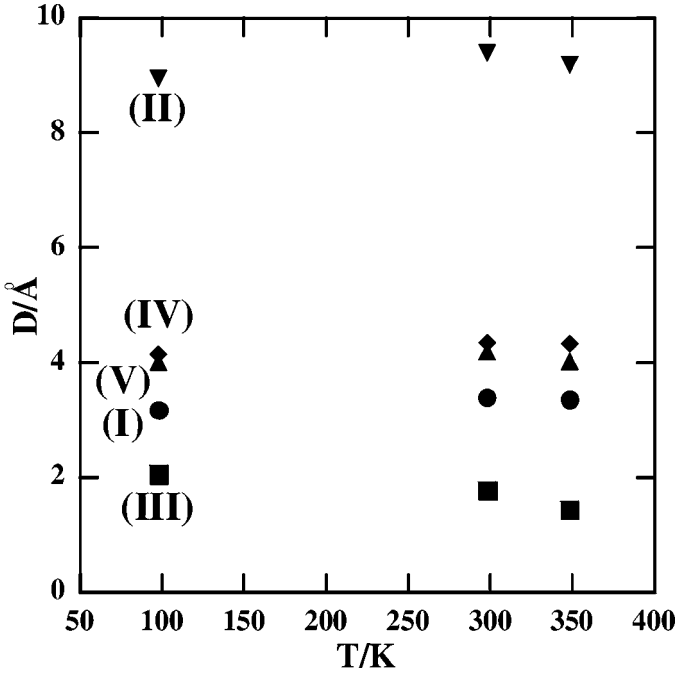

Figure 14
Temperature dependencies of the intermolecular contacts and packing geometries in a crystal of (2).

References

Altomare, A., Burla, M. C., Camalli, M., Cascarano, G., Giacovazzo, C., Guagliardi, A., Moliterni, A. G. G., Polidori, G. & Spagna, R. (1999). *J. Appl. Cryst.* **32**, 115–119.
Bondi, A. (1964). *J. Phys. Chem.* **68**, 441–451.
Castonguay, L. A. & Rappe, A. K. (1992). *J. Am. Chem. Soc.* **114**, 5832–5842.
Dunitz, J. D. & Bernstein, J. (1995). *Acc. Chem. Res.* **28**, 193–200.
Endo, T., Okubo, A., Kaneko, Y., Uehara, M., Tasai, H., Sato, A., Nikki, K., Nakagawa, N. & Kamei, S. (1982). *Bull. Chem. Soc. Jpn*, **55**, 2224–2232.
Gafner, G. (1960). *Acta Cryst.* **13**, 706–716.
Gafner, G. (1964). *Acta Cryst.* **17**, 982–985.
Kaftory, M., Botoshansky, M., Kapon, M. & Shteiman, V. (2001). *Acta Cryst.* B**57**, 791–799.
Katrusiak, A. (2001). *Acta Cryst.* B**56**, 872–881.
Molecular Simulations Inc. (2000). *Cerius*2, Version 4.2. Molecular Simulations Inc., San Diego, USA.
Rappe, A. K., Casewit, C. J., Colwell, K. S., Goddard III, W. A. & Skiff, W. M. (1992). *J. Am. Chem. Soc.* **114**, 10024–10035.
Rappe, A. K. & Colwell, K. S. (1993). *Inorg. Chem.* **32**, 3438–3450.
Schmidt, A., Kababya, S., Appel, M., Khatib, S., Botoshansky, M. & Eichen, Y. (1999). *J. Am. Chem. Soc.* **121**, 11291–11299.
Sheldrick, G. M. (1997). *SHELXL*97. University of Göttingen, Germany.
Steiner, T., Hinrichs, W. & Saenger, W. (1993). *Acta Cryst.* B**49**, 708–718.
Wilson, C. C. (2001). *Acta Cryst.* B**57**, 435–439.
Zamir, S., Bernstein, J. & Greenwood, D. (1994). *J. Mol. Cryst. Liq. Cryst.* **242**, 193–200.